VERIFICATION OF STIV ANALYSIS OF FLOOD DISCHARGE AT NAKANO OBSERVATORY IN THE OTA RIVER BY FLOW ANALYSIS USING ALB DATA

KEISUKE YOSHIDA
Okayama University, Okayama, Japan, yoshida.k@okayama-u.ac.jp

SHINYA NIGO
Chugoku Regional Development Bureau, MLIT, Hiroshima, Japan, nigo-s87bb@mlit.go.jp

SHIRO MAENO
Okayama University, Okayama, Japan, maeno@okayama-u.ac.jp

KOJI MANO
Pasco Corporation, Osaka, Japan, koonua2121@pasco.co.jp

MITSUTAKA NAKANO
Chugoku Regional Development Bureau, MLIT, Hiroshima, Japan, nakano-m87m@mlit.go.jp

ABSTRACT

Flooded river discharge has been measured using floating rods in Japan for reasons of cost-efficiency and feasibility. However, recent severe flood conditions that surpass planned severity pose new challenges for measurement with human works. For such practical issues related to river engineering, non-contact type measurement methods using cost-efficient devices and improved algorithms for flow analysis have been developed. These methods are anticipated for wider use in practical works of data acquisition for both river channel planning and disaster reduction. Nevertheless, their applicability must be verified and improved for various river conditions. We conducted flow measurements using space-time image velocimetry (STIV) analysis at Nakano Observatory in the Ota River in Japan during heavy rainfall in July 2018. Results revealed that the hourly discharge values obtained using an *H–Q* rating curve were overestimated by approximately 10 percent compared to those obtained using the present STIV analysis. Therefore, this study examined the accuracy of the present STIV analysis for river discharge estimation during flooding, using numerical simulation results and water level observations. First, we obtained data for both the topo-bathymetry and vegetation properties within the targeted reach from airborne laser bathymetry (ALB) measurement results. Secondly, we conducted numerical simulations of the flood flows using discharge hydrography of two kinds: The rating curve and the STIV analysis. Finally, we compared simulated water levels with observations made during flooding. Results demonstrated that the STIV analysis provides more accurate discharge data than data shown by the rating curve.

Keywords: Airborne laser bathymetry, river discharge observations, river flow analysis, space-time image velocimetry

1. INTRODUCTION

The river discharge record during flooding and the related rating curve constitute fundamental information for both river channel design and management. Traditionally, discharge in Japanese flooded rivers has been measured using floating rods dropped from a river bridge. This conventional method has been adopted nationwide because of cost-efficiency and feasibility. Nevertheless, it commonly requires many personnel to conduct fieldwork of several types in severe natural conditions: heavy rainfall and strong winds during rainy seasons and typhoons. Consequently, the conventional method provides limited data during flooding, thereby leading to a rating curve with low accuracy. The method also entails some difficulties to be addressed in terms of the river discharge measurement principle: e.g., remarkable drift of floating rods diverted from preferred paths. Recently, global warming phenomena have allegedly increased the frequency of devastating extreme flood occurrence. Accordingly, much more difficulty arises for ensuring the safety for personnel engaged in field measurements. Furthermore, fewer human resources are available for assignment for onsite flood-prevention tasks. That shortage of resources is related to the gradual change of Japan's industrial structure and working population. Such a background has posed new challenges for discharge measurements in flooded rivers.

To address such practical issues of river engineering, several measurement techniques have been developed (Costa et al., 2005; Fujita et al., 2007; Wang and Huang, 2005). Among them, non-contact type measurement methods with cost-efficient devices and improved algorithms for practical flow analysis are promising tools for river discharge measurements. These updated methods are anticipated for wider use in practical works for both river channel planning and disaster reduction. However, their applicability must be verified and improved for various river conditions. For this study, we conducted flow measurements using space-time image velocimetry (STIV) analysis at Nakano Observatory in the lower Ota River in Japan. Our targeted flood occurred during the heavy rainfall event in early July 2018. Then, we estimated hourly river discharge values during flooding. Next, we conducted numerical simulations of the flood flows using discharge hydrography of two kinds: the existing rating curve and STIV results. For numerical simulations, we especially obtained the river topo-bathymetry data, land-cover classification data, and vegetation attributes using airborne laser bathymetry (ALB) data. Subsequently, after comparing simulated water levels with observations during the flood, we examined the accuracy of the discharge hydrography using the present STIV analysis.

2. OTA RIVER DISCHARGE OBSERVATION DURING FLOODING IN JULY 2018

2.1 Study site and Ota River flooding in July 2018

The Ota River, a first-grade river in Japan, flows across Hiroshima prefecture into the Seto Inland Sea (Figure 1). The 3.5 km long targeted river reach is located approximately 17 km upstream from the river mouth (as portrayed in Figures 8 and 9). In early July 2018, the western part of Japan, including this prefecture, experienced a heavy rainfall event. The record-setting long-duration rainfall was observed during July 5–7, causing massive flooding of rivers throughout the prefecture. We observed two recognizable floods in the lower Ota River during this rainfall event. The first larger flood is targeted for consideration in this study. The peak period of the targeted flood occurred at night on July 6–7.

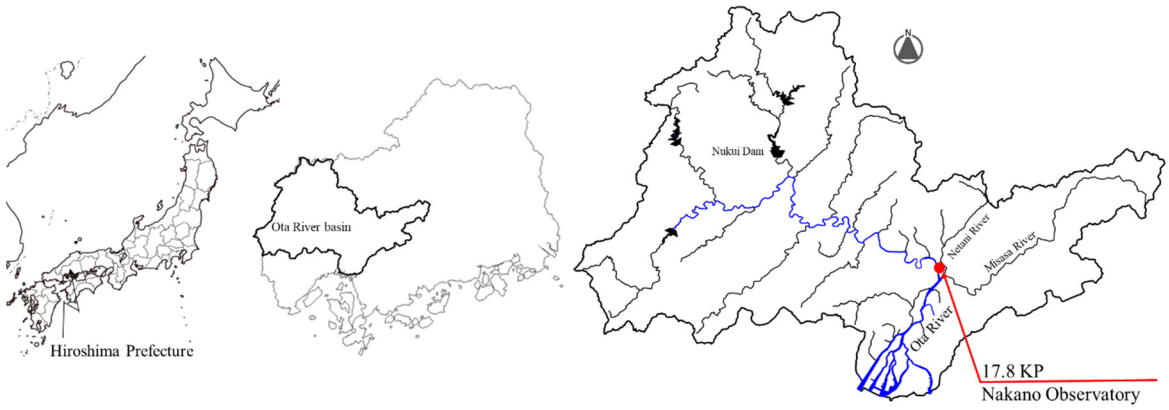

Figure 1. Study site: Nakano Observatory and Ota River basin in Hiroshima Prefecture, Japan.

2.2 Discharge observation for Ota River flooding

River discharge in the targeted reach was measured at Nakano Observatory (17.8 KP cross-section), as shown in Figures 1 and 2. Hereinafter, the kilometer post (KP) value represents the longitudinal distance (kilometer, km) from the river mouth. At this hydraulic station, the floating rods are dropped from the rope spanned across the river for discharge measurements during flooding. Furthermore, two closed-circuit television (CCTV) cameras of infrared type (FC-618-35 mm-30 Hz; FLIA Systems Japan, Inc.) were installed on both banks of the targeted river cross-section. The setup specifically considers operation at night and also eliminates blind areas. These cameras recorded images for the discharge measurement during Ota River flooding in 2018. During flooding, no rainfall and negligible wind were recorded around the site, based on reports from field workers for discharge measurements using floating rods. Figure 3 depicts the targeted cross-section and setting of camera angles. In this figure, the italic number signifies the subarea for the river discharge calculation.

Figure 4 presents a typical image of the left-side camera, recorded at 19:00 on July 6 at the targeted cross-section during flooding in 2018. The corresponding surface flow velocities were superimposed on the figure. The velocities were estimated using software for STIV analysis (KU-STIV; Be-system, Inc.). By default, this software automatically analyzes the surface velocities using STIV analysis (Fujita et al., 2007). For preliminary preparation for the STIV analysis, geometric correction was conducted for the oblique camera images. It uses survey results for several targeted objects placed in the river bed during a normal water stage. In Figure 4, green lines represent the search lines for STIV analysis. Red vectors show the surface velocity vectors. The streamwise length of the lines was set as 10 m. The analytical period for velocity estimation was assigned as 60 s (Figure 6). The velocity vectors at sub areas (No. 12 and No. 13; Figure 3) are not considered by the left-side camera.

The infrared camera images were clearly recorded for the STIV analysis. Additionally, no image degradation attributable to raindrops on the camera lens was recognized during recording.

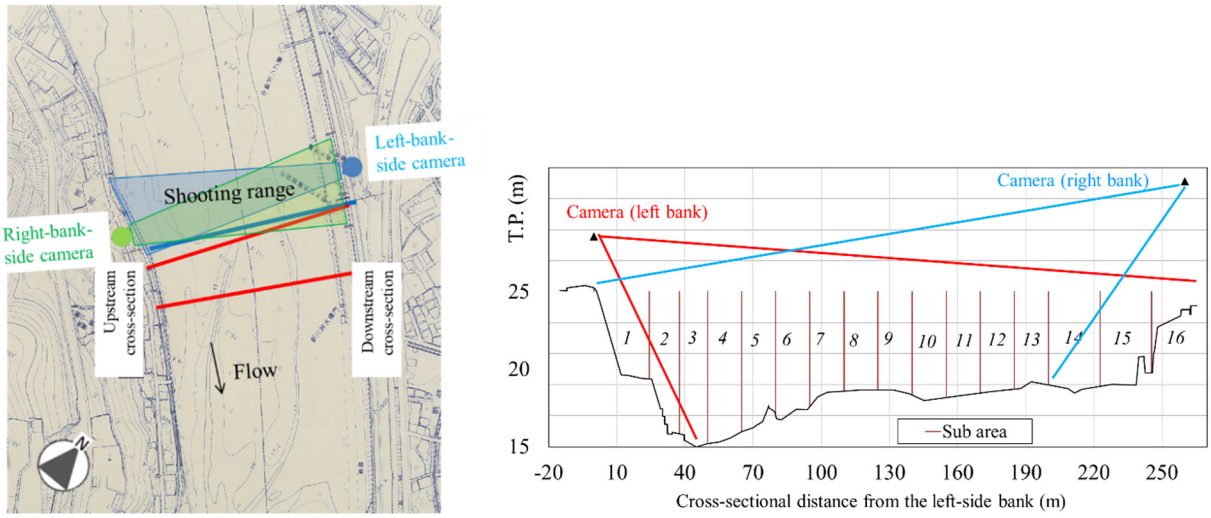

Figure 2. (left) Targeted cross-section and observation setup at Nakano Observatory (17.8 KP): red lines, cross-sections for discharge observations using floating rods; blue and green areas, shooting ranges of two cameras.

Figure 3. (right) Setting of camera angles for image recording at the targeted cross-section (17.8 KP).

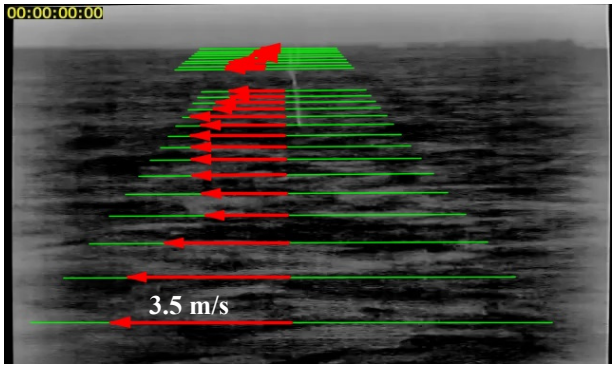

Figure 4. Left-side infrared camera image superimposed with corresponding STIV result at 19:00 on July 6 at the targeted cross-section: green lines, searching lines for STIV analysis; red vectors, surface velocity vectors.

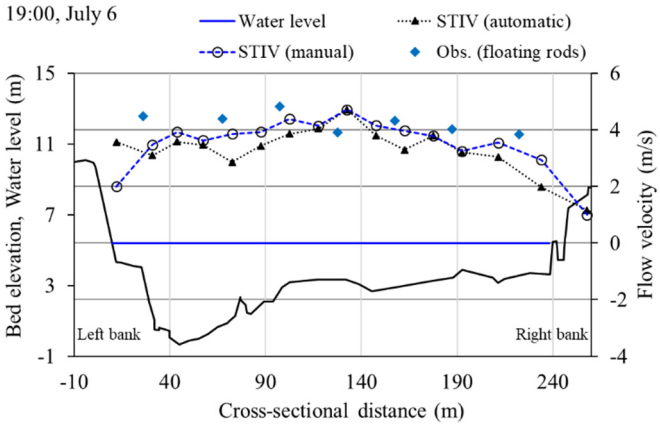

Figure 5. Surface velocities at the targeted cross-section (Nakano Observatory, 17.8 KP).

2.3 Manual modification and verification of the discharge values using STIV analysis

The river discharge was estimated hourly at the targeted cross-section. For estimation, we used both the surface flow velocity and water depth at each subarea (Figure 3). For this study, the correction coefficient was set as the standard value of 0.85 for converting the surface velocity to the subarea-averaged velocity. Figure 5 shows the STIV result of surface velocities at the targeted cross section at 19:00 on July 6. For reference, the

observation results obtained using floating rods are added to the figure. Results show that the discharge values are mostly underestimated by automatic STIV analysis. Therefore, we manually verified the surface velocity values. Figure 6 presents an example of the STI image and analyzed surface velocities: red line, automatic results; blue line, manual results. Manual results are also added to Figure 5. Results show that the discharge values using the present STIV analysis with manual modification are roughly consistent with observations compared with those without modification. This result might derive from mixing of the unsteady turbulent flow and gravity wave occurring in the river section during flooding. Therefore, the STIV results cannot be computed in real-time under the current system deployed at this station

We completely checked the present STIV results with manual modification during the targeted flood period. Figure 7 presents the hourly results of discharge hydrography using the STIV analysis. We added the field observation results obtained using floating rods and the rating curve using a stage–discharge (H–Q) relation. As earlier studies described clearly (e.g., Harada et al., 2007), the discharges obtained using the floating rods and the related rating curve might be overestimated by approximately 10 % to 20 % in the present flood event. The present STIV results with manual modification are roughly consistent with the observation results obtained using floating rods, compared with the rating curve. For this work, accuracy of the river discharge using the present STIV result is ascertained in the following section describing flooded river simulations.

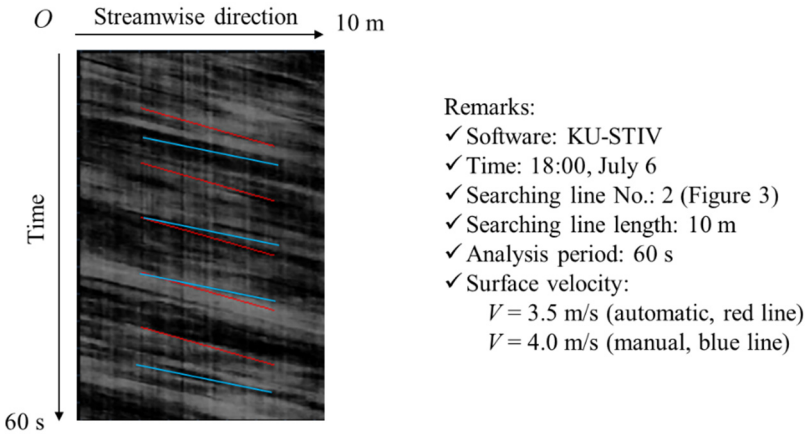

Figure 6. STI image superimposed with analyzed velocities.

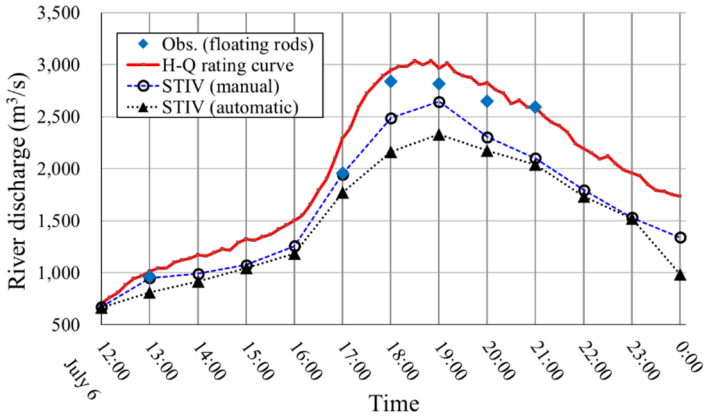

Figure 7. River discharge hydrograph at Nakano Observatory during flooding during 12:00–24:00 on July 6.

3. ALB DATA COLLECTION

3.1 Targeted domain and specifications of ALB measurements

Topo-bathymetric surveys were conducted in the targeted reach from 15 KP to 21 KP during a normal water level on November 16–18, 2018 after flooding. For these surveys, we used a specific ALB device (Leica Chiroptena II; Leica Corp.). Flight operations were conducted several times to achieve overlapping coverage of the targeted area under leaf-less and clear water conditions. The surveys were conducted using near-infrared and green lasers mounted on an aircraft. The device uses green light to probe underwater (bottom) surfaces because green light penetrates into bodies of water to some degree. The near-infrared light device detects the terrain surface and overland vegetation because the air–water interface reflects the near-infrared light.

The device provides raw ALB data comprising a set of laser points, or a point cloud recorded with local Cartesian coordinates. The global coordinates for use were specified using global navigation satellite system

(GNSS) data. Through data processing, the point cloud was analyzed using a full-waveform technique (Zhu et al., 2015). This technique especially accommodates distinction of ground hits from object surface hits (e.g., vegetation). Furthermore, the water edge separating overland and underwater surfaces was identified from image information of aerial photographs taken simultaneously during ALB measurements. The detailed information is described in Yoshida et al. (2019) related to both instrument specification and data processing for ALB measurements.

3.2 River topo-bathymetry, land use type classification, and vegetation attributes

Figure 8 shows ALB data of a bathymetry contour map of the target domain. In this figure, Tokyo Peil (T.P.) is the data level used throughout this study. It represents the average sea level of Tokyo Bay in Japan. The figure was drawn using ALB data with a space resolution of 2 m. For reference, we compared the bed elevation using ALB data with the ground survey obtained after the 2018 flooding at the targeted cross-section. The present ALB data are consistent with the ground survey data with average accuracy of approximately 10 cm. That spatial scale corresponds to the gravel size observed onsite. Therefore, the present ALB data are used for numerical simulations of Ota River flooding in 2018, as described hereinafter.

Figure 9 shows the land use type using ALB point cloud data for the targeted river reach. We inferred the land use type on gravel bars and floodplains using GIS software (ArcGIS) using supervised classification. For this study, we classified the river terrain into three kinds in terms of flow resistance during flooding: herbaceous vegetation, woody vegetation, and non-vegetated bed (dry or wetted). This determination was made based on aerial photographs. In addition, vegetation heights were checked using field observations in several subregions.

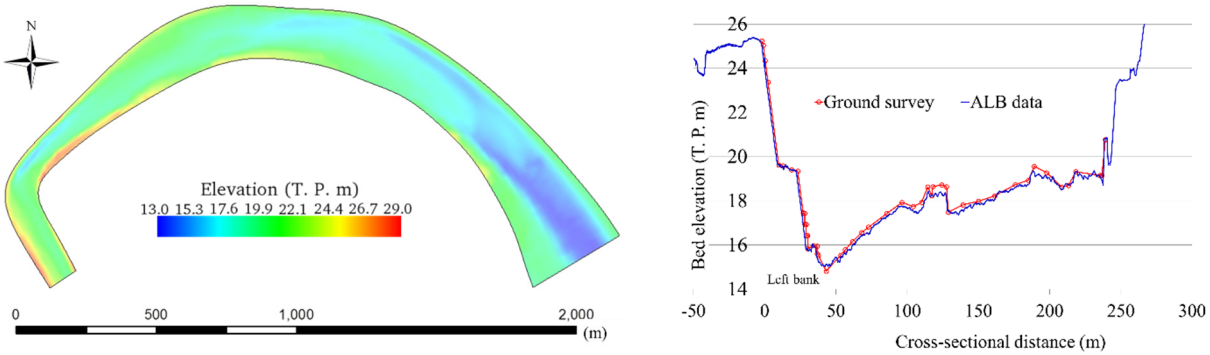

Figure 8. ALB data of a topo-bathymetry contour map of the target domain for numerical simulations (left) and verification of ALB data for the bed survey at 17.8 KP section (right).

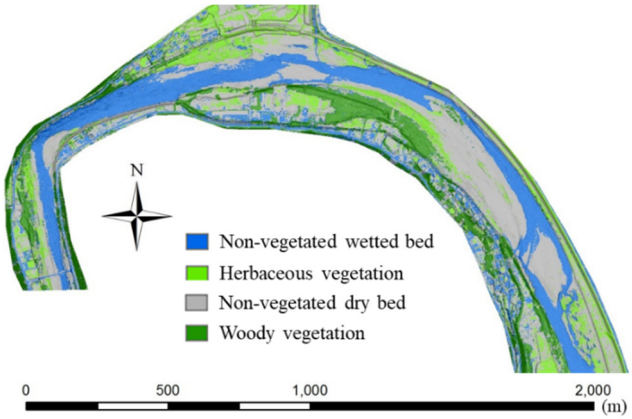

Figure 9. Land cover classification for the targeted river reach using the ALB data obtained after flooding in 2018.

4. FLOODED RIVER SIMULATIONS USING ALB DATASET

4.1 Governing equations and numerical solution

Numerical simulations were conducted for Ota River flooding in July 2018. The targeted domain for the simulations includes the Ota River reach from 16.7 KP to 20.2 KP (Figure 10). Only one hydraulic station (Nakano Observatory) operates in the targeted domain for water level measurements. River discharge Q was estimated at the station using the stage–discharge (H–Q) relation. Furthermore, the water levels at three locations (16.7 KP, 18.4 KP, and 19.8 KP in Figure 10) were measured using simplified instruments designed for use only during flooding. The simulated water levels were compared with these observed results.

We used the depth-averaged two-dimensional flow solver (IRIC, Nays2DH, ver.3.0) for the flood simulations. Recently, this solver has been widely used and fully validated for flood flow simulations worldwide. In this solver, a shallow-water hydrodynamic model using the boundary-fitted coordinate system is used for practical flood flow simulations. Dependent flow variables for this study are the local values of water depth and depth-averaged flow velocity. To model the surface friction on a non-vegetated riverbed, the hydrodynamic roughness is evaluated using Manning's formula. The modelling of flow resistance attributable to vegetation is described in the following subsection. The governing equations were discretized in a staggered mesh using the finite difference method. Time development of the flow variables was computed explicitly using the first-order Euler scheme. Spatial derivatives were discretized using the second-order central scheme, except for advection terms, which were discretized using the CIP scheme. The boundary conditions of both the discharge and water level were set at the targeted river reach ends based on flooding records.

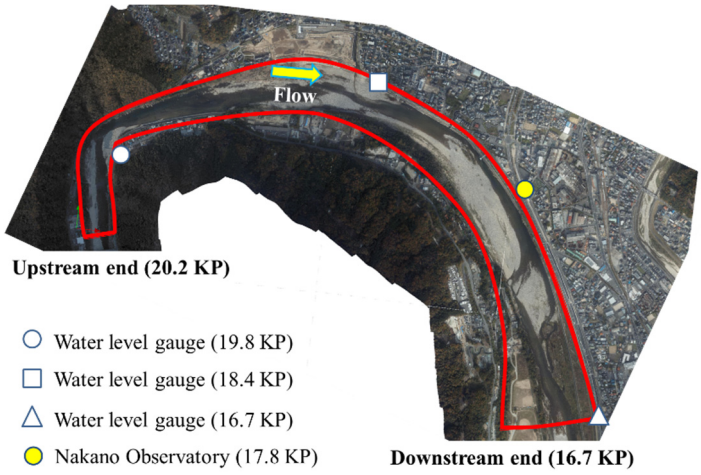

Figure 10. Targeted river reach and water levels measured at four points during flooding.

4.2 Drag force caused by vegetation establishment

We considered the local drag force attributable to woody vegetation establishment in the governing equations as a source term. For physical modelling, we considered the similarity of hydrodynamic forces exerted on rigid cylinders (e.g., Sun et al., 2010) for flow resistance attributable to vegetation. In this framework, we used non-uniform ALB data of vegetation attributes for the drag force estimation. Formulation for the woody species can be conducted using the $0.5\rho\lambda C_D l_{\min} u^2$ term. In this expression, ρ denotes the water density, λ represents the vegetation density for willows, C_D is the drag coefficient, $l_{\min}= \min\{h, l\}$ signifies the minimum value of vegetation height l and local flow depth h, and u stands for the local flow velocity.

4.3 Numerical conditions and test cases

We conducted unsteady numerical simulations of the earlier described model as follows. The time increment was 0.007 s. The increment was adjusted to allow for numerical stability. The computational mesh consisted of 350 × 16 cells, with 350 cross-sections in the longitudinal direction and 16 nodes in each cross-section. The numerical mesh sizes were approximately 10–15 m. The computation period was 12 hr from 12:00 on 6 July through 24:00 on that day in 2018. Overall, we observed little bed deformation in the targeted domain during flooding. Therefore, for simplicity, this study did not incorporate deposits or erosion of bed materials.

The value of Manning's roughness coefficient was assigned as 0.028 (from 16.7 KP to 19.8 KP) and 0.032 (from 19.8 KP to 20.2 KP). Those values were found based on reference to earlier reports for the Ota River management tasks. The river characteristics (bed slope, bed material size, etc.) and river landscape at upstream sections from the 19.8 KP differ from those at downstream sections in the Ota River. These roughness values allow for the total flow resistance attributable to the riverbed under past larger floods in the targeted reach, not considering the woody vegetation establishment. The vegetation density distribution for woody vegetation was estimated using an empirical value proposed by earlier studies (Maeno et al., 2005; Shimizu et al., 2000). Small herbaceous vegetation was visible as distributed over the study site before flooding. For simplicity, the herbaceous vegetation was not considered for drag force estimation for this study.

We set up two cases for numerical simulations, as shown in Table 1. These two cases differ in the dataset of the discharge hydrography for numerical simulations. For Case 1, we used the stage–discharge (H–Q) relation with the water levels observed every 10 min at Nakano Observatory during flooding. In contrast, we used the hourly results of the STIV analysis for CCTV images captured at Nakano Observatory for Case 2 (Figure 8). For both cases, the discharge data were interpolated linearly in conformity to the time increment of numerical simulations.

Table 1. Discharge conditions for numerical tests.

	Discharge hydrograph	Approximate value of peak discharge during flooding (m^3/s)
CASE 1	Stage–discharge relation with water levels every 10 min observed during flooding at Nakano Observatory	3000
CASE 2	Hourly discharge obtained using the STIV analysis for CCTV images at Nakano Observatory	2600

4.4 Simulation results for verification of the discharge hydrography during flooding

Figure 11 presents simulation results of water depth distribution and velocity vectors for Case 2. These simulated results correspond to flow fields in the initial condition (left) and the peak stage of flood (right, 19:00, July 6). During flooding, the water edge varies over time. The right-side downstream area is not inundated throughout the flood because of high bed elevation. The simulated velocity vectors are simulated without unphysical oscillation. Overall, the flow field during flooding is simulated reasonably because of the accurate representation of the topo-bathymetry of the targeted river reach using ALB dataset (Figure 8).

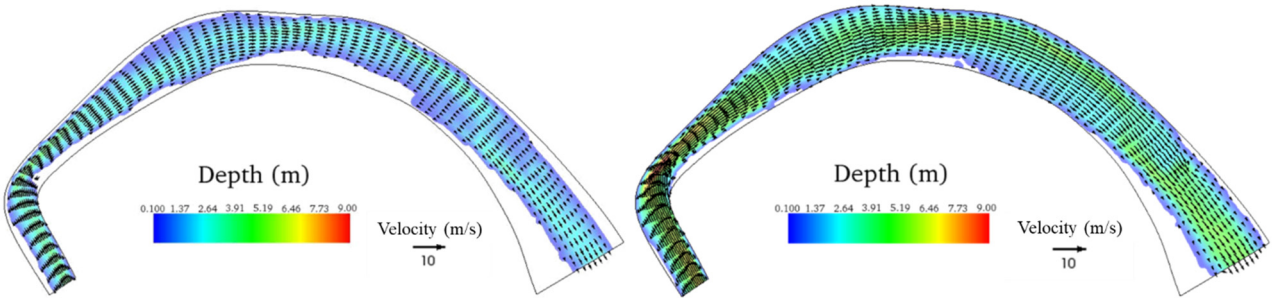

Figure 11. Simulated results of water depth contour and velocity vectors for Case 2: left, at 12:00; right, at 19:00.

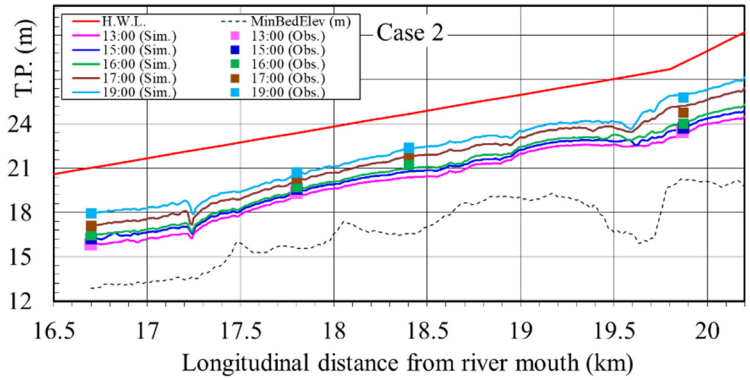

Figure 12. Longitudinal distribution of simulated water levels along the reach for Case 2 with observation: H.W.L., high water level; MinBedElev, minimum bed elevation; Sim., simulation results; Obs., observation results.

Figure 12 presents a comparison of the longitudinal distribution of observed water levels with simulated water levels at five points of time during the rising flood stage. The red line represents the high water level (H.W.L.) designated for protection against the flooding targeted in the Ota River. The dotted line shows the longitudinal profile of the bed level averaged along each cross-section. Profiles of the simulated water levels are approximately consistent with the observations.

Figure 13 presents a comparison of time variation of observed water levels with simulated water levels at three locations: 17.8 KP (left-side bank), 18.4 KP (left-side bank), and 19.8 KP (right-side bank) for Case 1 and Case 2. Results demonstrate that the simulated water levels in Case 1 are overestimated by an average of approximately 50 cm compared with observations. Simulated results obtained for Case 2 are consistent with observations. Therefore, the discharge hydrograph using the present STIV results reasonably represents the Ota River flooding in 2018.

5. CONCLUSIONS

This study produced flow measurements using STIV analysis of CCTV images recorded at Nakano Observatory during the 2018 Ota River flooding. Results indicated that the discharge values obtained using the existing rating

curve were overestimated by approximately 10 percent compared to those obtained using the present STIV analysis, as earlier studies (e.g. Harada et al., 2007) describes clearly. Given that background, we investigated the accuracy of the STIV analysis in operation at Nakano Observatory for flooded river discharge estimation. We used both numerical simulation results and water level observations. First, we obtained river data, which include topo-bathymetry, land use type, and vegetation attributes in the targeted reach by airborne laser bathymetry (ALB) measurement results. Subsequently, we conducted numerical simulations of the flood flows using discharge hydrography of two kinds: the rating curve and the STIV analysis. Results demonstrated that the STIV result for the CCTV images provides more accurate discharge data than those of the rating curve. For this work, we used the standard value (0.85) for the correction coefficient in the present STIV system. In our future work, we will examine the uncertainty of the coefficient for more flood events with different discharges. Furthermore, we will check the STIV-derived discharge values, in comparison with other accurate measuring methods including the acoustic Doppler current profiler (ADCP).

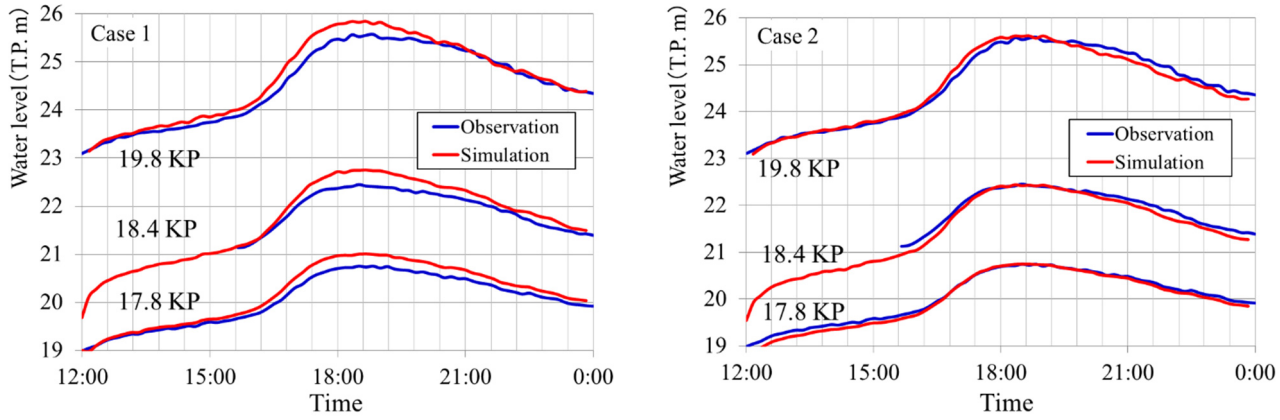

Figure 13. Time variation of observed and simulated water levels along the reach: left, Case 1; right, Case 2.

ACKNOWLEDGMENTS

This research was supported in part by the Electric Technology Research Foundation of Chugoku and in part by the Takahashi Industrial and Economic Research Foundation. This work was also supported in part by JSPS KAKENHI Grant No. 18K04370. The authors appreciate the Chugoku Regional Development Bureau, Ministry of Land, Infrastructure, Transport and Tourism for offering all observation data measured at hydraulic stations along the Asahi River and Hyakken River.

REFERENCES

Costa, J. E., Cheng, R. T., Haeni, F. P., Melcher, N., Spicer, K. R., Hayes, E., Plant, W., Hayes, K., Teague, C., and Barrick, D. (2006). Use of radars to monitor stream discharge by noncontact methods. *Water Resources Research*, 42(7):W07422.

Fujita, I., Watanabe, H., and Tsubaki, R. (2007). Development of a non-intrusive and efficient flow monitoring technique: The space-time image velocimetry (STIV). *Intl. J. River Basin Management*, 5(2):105-114.

Harada, Y., Nihei, Y., Sakai T., and Kimizu, A. (2007). Fundamental study on measuring accuracy for flood discharge with floats, *Annual J. Hydraulic Eng*., 51:1081-1086. (in Japanese)

IRIC-UC (2010). IRIC Software, Nays2DH, https://i-ric.org/.

Maeno, S., Watanabe, A., and Fujitsuka, Y. (2005). Improvement of modeling of flow analysis using easily obtained vegetation characteristic. *Journal of Hydraulic, Coastal and Environmental Engineering*, II-73, 91-104. (in Japanese)

Shimizu, Y., Kobatake, S., and Arafune, T. (2000). Numerical study of the flood-flow stage in gravel-bed river with the excessive riverine trees. *Annual J. Hydraulic Eng*., 44:819-824. (in Japanese)

Sun, X., Shiono, K., Rameshwaran, P., and Chandler, J. H. (2010). Modelling vegetation effects in irregular meandering river. *J. Hydraulic Research*, 48(6):775-783.

Wang, F. and Huang, H. (2005). Horizontal acoustic Doppler current profiler (H-ADCP) for real-time open channel flow measurement: Flow calculation model and field validation, Proc. *XXXI IAHR World Congress*, 319–328.

Yoshida, K., Maeno, S., Ogawa, S., Mano, K., and Nigo, S. (2019). Estimation of distributed flow resistance in vegetated rivers using airborne topo-bathymetric LiDAR and its application to risk management tasks for Asahi River flooding. *Journal of Flood Risk Management*, e12584. (in print)

Zhu, L., Subas, C., Tachibana, K., and Shimamura, H. (2015). Methodology development on full-waveform aerial LiDAR data analysis. *J. Japan Society of Photogram. and Remote Sens*., 54(1):4-19. (in Japanese)